

SILICON PRODUCTION, REFINING, PROPERTIES, AND PHOTOVOLTAICS

Finite Element Analysis and Techno-economic Modeling of Solar Silicon Molten Salt Electrolysis

ADITYA MOUDGAL $^{\circ}$, 1,4 SARAT BUASAI, 2,5 YI JIE WU, 2,6 ALEXANDER MCMAHON, 2,7 JACOB M. HAZERJIAN, 2,8 VICKY LUU, 2,9 ARIANA LY, 2,10 MOHAMMAD ASADIKIYA $^{\circ}$, 1,11 ADAM POWELL $^{\circ}$, 1,12 UDAY PAL $^{\circ}$, 3,13 and YU ZHONG $^{\circ}$

1.—Materials Science and Engineering Program, Department of Mechanical Engineering, Worcester Polytechnic Institute, 100 Institute Rd., Worcester, MA 01609, USA. 2.—Department of Chemical Engineering, Worcester Polytechnic Institute, 100 Institute Rd., Worcester, MA, USA. 3.—Division of Materials Science and Engineering, Boston University, 730 Commonwealth Ave, Boston, MA, USA. 4.—e-mail: amoudgal@wpi.edu. 5.—e-mail: sbuasai@wpi.edu. 6.—e-mail: ywu9@wpi.edu. 7.—e-mail: amcmahon@wpi.edu. 8.—e-mail: jhazerjian@wpi.edu. 9.—e-mail: vluu@wpi.edu. 10.—e-mail: aly@wpi.edu. 11.—e-mail: masadikiya@wpi.edu. 12.—e-mail: acpowell@wpi.edu. 13.—e-mail: upal@bu.edu. 14.—e-mail: yzhong@wpi.edu

A new process is presented for low-cost one-step production of pure solid silicon from natural quartzite by molten salt electrolysis. At a process temperature of 1100°C, a techno-economic model including detailed mass and energy balances estimates energy consumption below 15 kWh/kg, with operating cost of \$1.74/kg and capital cost around \$10,500 per t/a (tonne annually) of production capacity for a 160,000 t/a plant. Use of an inert solid oxide membrane anode results in a pure oxygen by-product and no direct emissions. Finite element analysis estimates the current density distribution and total current to inform the design of slab-shaped solid silicon cathodes.

INTRODUCTION

Abundance, low cost, and good photovoltaic (PV) efficiency have made silicon the dominant solar cell material for the past 30 years, and it will likely remain so for at least the next 10 years as well. A customer discovery exercise conducted by the authors in 2020 indicated high sensitivity to cost for polycrystalline silicon ("polysilicon") raw material with sufficient purity for efficient PV cells. Polysilicon production begins with carbothermic reduction of silica, which takes ≥ 99.7% pure SiO₂ and introduces impurities, creating 98% pure metallurgical grade (MG) silicon. The Siemens process refines MG silicon to make most of the world's 450 kt/a PV polysilicon by trichlorosilane synthesis, distillation, and chemical vapor deposition. This process is energy-intensive and costly, has inherent safety issues, ^{2,3} and is slow to scale. Although the demand shock of 2007-2008 is far behind us, the increases in polysilicon prices in early 2020 were

attributed to environmental issues and long lead time for plant construction.⁴ These issues and advances in PV efficiency at lower Si purity⁵ have motivated the development of simpler processes for purifying MG silicon using fluidized beds,^{6,7} liquid metals,^{8,9} slags,^{10,11} and electrorefining.^{12–15} But despite decades of development, these have only reached 15 kt/a to 20 kt/a (kilotonnes annually) production for solar cells.

Molten salt electrolysis could reduce quartzite directly to silicon in a single step, with inherent purification and zero direct emissions, bypassing the carbothermic and Siemens process steps. ^{16,17} To date, investigations have used cathode electro-deoxidation, ^{18,19} potassium fluorosilicate (K₂SiF₆) reduction, ^{15,20–22} and reduction with liquid aluminum, ^{23,24} copper, ^{14,25} nickel, ²⁶ gallium ²⁷ and zinc ²⁸ reactive cathodes to avoid SiC formation. But low SiO₂ solubility in molten chlorides, side-reactions making volatile SiCl₄ and SiF₄, high viscosity and low conductivity caused by silicate polymerization, contamination by carbon anodes and their

impurities, and trapped salts in the product have prevented scale-up and commercialization of this approach.

Recent molten salt chemistry advances promise to solve several of these problems. 29–31 Starting with CaF2-MgF2 eutectic with low volatility, high mobility, and a wide electrochemical stability window, the electrolyte adds CaO to provide O2- ions which increase the solubility of SiO2, break up silicate polymer networks, and prevent SiF₄ volatilization. Though a carbon anode is not practical, a yttriastabilized zirconia (YSZ) solid oxide membrane (SOM) can protect an inert anode. 32,33 YSZ stability in the electrolyte requires two characteristics of the solid and liquid electrolytes: similar Y³⁺ ion activity to prevent leaching, and similar optical basicity to minimize dissolution and ion exchange. The electrolyte thus contains (by weight): 45.6% CaF₂, 36.4% MgF₂, 9.0% CaO, 5.0% SiO₂, and 4.0% YF₃, in decreasing order. SiO2 reduction using this electrolyte with a liquid tin cathode produced tin-silicon alloy which formed millimeter-scale silicon crystals when cooled;²⁹ others have shown that solar silicon can be grown by tin-silicon solidification.³⁴

Proposed here is a silica electrolysis process using this bath chemistry at 980°C to -1200°C to produce solid silicon. This can potentially utilize both electrochemical refining and low solid silicon partition coefficients in a single process. To prevent dendrite formation, a subset of cathodes periodically reverses to anodic potential, dissolving incipient roughness. To give 1 schematically shows the reaction and switching scheme.

This paper describes a modeling study based on this proposed process and current practice in aluminum smelting. It begins with a brief description of plant and cell operation. Mass and energy balances determine material and energy requirements and costs. Finite element analysis (FEA) of cell components estimates current density, electrolyte resistance, and temperature change, and illuminates design constraints. In particular, electrode and

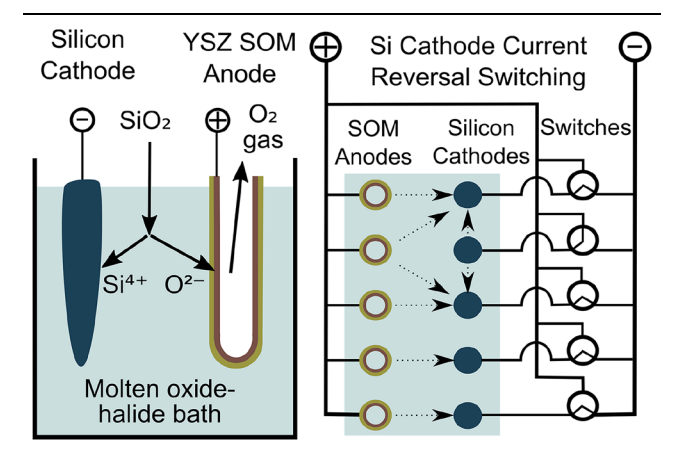


Fig 1. Schematic diagrams of the proposed process (left) and switching scheme for periodically reversing cathode polarity on a high-current DC bus. Si⁴⁺ represents oxidation state; silicon will be present in complex anions.

electrolyte conductivities impose constraints on the electrode design. With no gas lift stirring, magneto-hydrodynamics (MHD) is likely the best stirring mechanism, and FEA estimates molten salt flow velocity and resulting deposition profile.

SILICON CELL AND PLANT PRELIMINARY DESIGN

Figure 2 shows a schematic and preliminary design of a 100-kA silicon electrolysis cell. It uses vertical electrodes with 0.2 A/cm² to 0.3 A/cm² cathode current density and 0.5 A/cm² anode current density, resulting in a production rate slightly higher than Hall-Héroult aluminum smelting on a cell footprint area basis. The container may be constructed of zirconia, as the electrolyte is designed to minimize zirconia corrosion, or it may use a frozen electrolyte side-wall and bottom similar to Hall-Héroult. In the current 300-kA design, the slab cathodes are 2.5 m long and 1.2 m deep, and start 2–8 cm thick, then grow outward to nearly 12 cm to 18 cm thickness before removal. SOM anodes include 3 cm outer diameter, 2.6 cm inner diameter (2 mm thick) closed-end YSZ SOM tubes, with an oxygen-evolving porous ceramic anode such as lanthanum nickelate (LaNiO₃) inside, and nickel or another high-conductivity oxidation-resistant alloy current collector, such that oxygen flows up the center of each tube. They are immersed 89 cm into the molten salt electrolyte and placed in rows spaced with centers 6 cm apart.

The process operating temperature window is from 980°C to 1200°C, limited at the low end by the CaF₂-MgF₂ eutectic temperature and at the high end by volatility, materials, and other practical considerations. At higher temperatures, materials such as silicon, molten salt, and zirconia have higher conductivities, improving energy efficiency, but the growing silicon cathode may incorporate impurities at higher concentrations. Models shown here use a cell temperature of 1100°C.

The large direct-current (DC) bus can create a large magnetic field which interacts with current in the molten salt to create Lorentz forces and stirring. In a Hall-Héroult plant, stirring is dominated by CO₂ gas lift from bubbles created on the anodes, and Lorentz force is a problem. In this cell without gas lift stirring, thermal buoyancy is too weak and mechanical stirring is impractical, so Lorentz force is necessary for distributing SiO2 raw material throughout the cell and reducing mass transfer overpotentials. The ideal external magnetic field direction is vertical, as vertical magnetic field and horizontal currents drive horizontal flows parallel to silicon plate cathodes, and minimize forces on vertical electrodes within the cell. The current bus and cell arrangement shown schematically in Fig. 2, with electrolysis cells in a potline located between large bus bars roughly in the plane of the cells, achieves this vertical magnetic field.

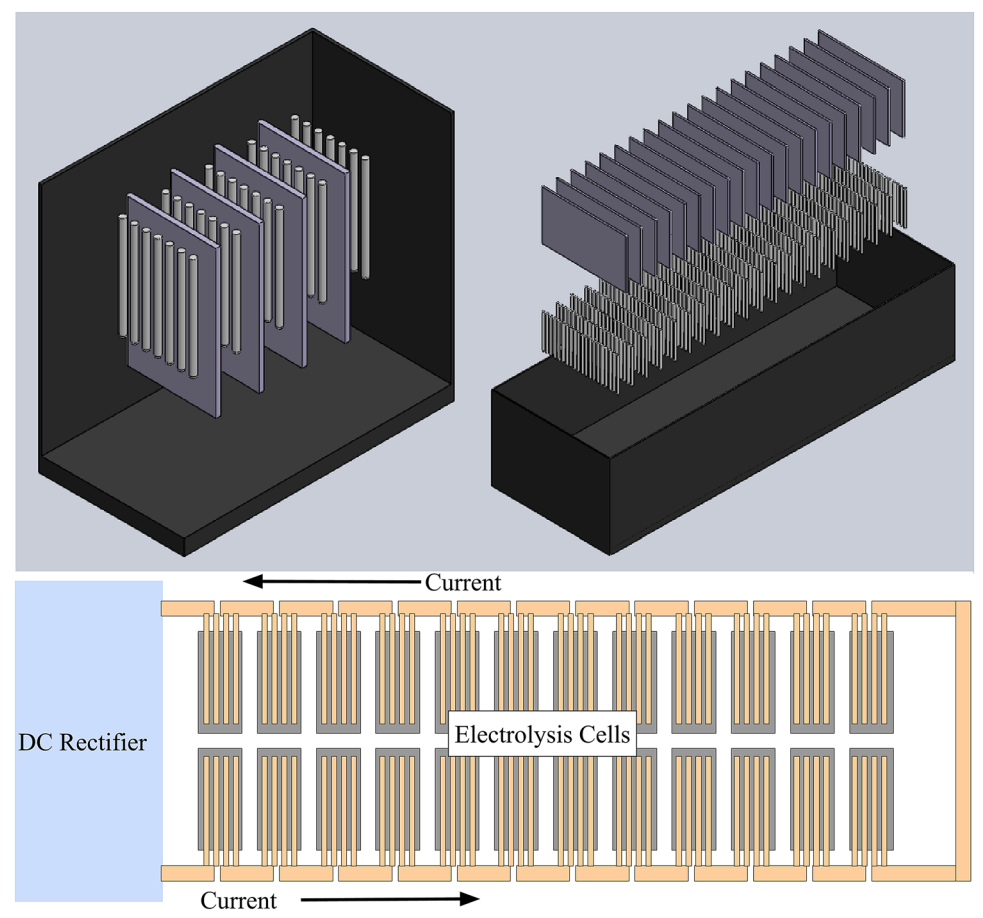


Fig 2. Preliminary cell design: (left) anode tube and cathode slab design schematic, (right) exploded view of a 100-kA cell roughly 5 m long \times 2 m wide with 441 \times 225 A tubular anodes and 20 \times 5 kA slab cathodes, (bottom) current bus and cell layout top view for vertical magnetic field and MHD stirring.

A plant with this design can use the high current bus, silica raw material distribution, and exhaust gas treatment design elements which are similar to a Hall-Héroult aluminum plant. Indeed, it may be possible to retrofit an idle aluminum smelter to dramatically reduce plant construction cost.

MODELING METHODS AND TOOLS

Techno-economic Modeling

The cost model uses the US Department of Energy ARPA-E METALS Tool techno-economic analysis spreadsheet v1.0,³⁶ which is included online as a supplementary document. This modeling tool includes:

- A mass balance calculating element-by-element balances with raw material costs and sales revenues
- Capital costs such as equipment with associated utility costs
- Estimates for other operating costs
- Estimation of total energy use and direct CO₂ emissions per unit of metal produced
- A financial model with return on investment

This study adds a linear equation system to the ARPA-E METALS Tool and a solution for calculating compositions and flow rates of five coupled streams: raw material and bath in, and silicon, oxygen, and bath out. This results in an inputoutput balance for all 13 model elements, which is perfect within the precision limits of the spreadsheet as verified by the original spreadsheet's streams and compositions sheets. The mass balance uses silica raw material purity and price data. It assumes that alumina is the most significant silica impurity, and adds new CaF₂, MgF₂, CaO, and Y₂O₃ to keep the alumina concentration in the bath low. Anodes are not included in the mass balance at this point.

This study also adds to the ARPA-E METALS Tool an energy balance following Ref. 38 which totals the reduction potential and ohmic overpotentials to estimate electrical energy input per coulomb of charge passed *V* as follows:

$$V = -\frac{\Delta G}{nF} + \Sigma \frac{J_i L_i}{\sigma_i} + 2\sqrt{L_{el}T\Delta T}$$
 (1)

where ΔG is the free energy of formation of SiO₂, n = 4 is the number of electrons transferred in the reaction, F is Faraday's constant, J_i , L_i , and σ_i are the current density, resistivity, and thickness of component i (YSZ SOM and molten salt), L_{el} is the Wiedemann-Franz constant, T is absolute temperature, and ΔT is the temperature difference. The last term is the electrical potential across two electrode leads designed for minimal total electrical and thermal losses in a monopolar high-temperature electrolysis cell.³⁸ Thermodynamic data are obtained from NIST JANAF tables.³⁹ Temperaturedependent conductivity data for the molten salt and YSZ are from Villalón³¹ and Krishnan,⁴⁰ the latter of which used 6 mol.% YSZ and could be increased by using 8 mol.% YSZ and/or advanced sintering.⁴¹ The YSZ SOM thickness is 2 mm, and the anodecathode distance with liquid electrolyte is 3 cm thick; in both, the current density is 0.5 A/cm². Cathode resistance is not included in this estimate. This one-dimensional (1-D) model acts as useful verification for the finite element analysis described below.

The energy balance then calculates the thermal energy requirement per kilogram of silicon product, including the temperature-dependent enthalpy of formation of SiO_2 , total electrical and thermal losses through the leads, and energy to heat SiO_2 raw material to the cell temperature:

Energy =
$$-\Delta H_f + 4nF\sqrt{L_{el}T\Delta T} + \int c_n dT$$
 (2)

In a self-heated cell, the thermal energy use should be lower than the equivalent electrical energy input calculated in Eq. 1: Energy < nFV, and the excess energy is lost as heat. Compared with Hall–Héroult cells with inert anodes, the theoretical energy use ΔH_f is 9.02 kWh/kg for silicon versus 8.62 kWh/kg for aluminum (about 5% higher), and the productivity at perfect Faraday efficiency is 262 g/kAh for silicon versus 336 g/kAh for aluminum (about 22% lower), so the processes are highly comparable.

The cost model uses prices of \$150/t for 99.8% pure SiO_2 , 37 \$150/t for CaO, \$400/t for CaF₂, \$1000/t for MgF₂, and \$5000/t for Y₂O₃, which is about half as expensive per unit of yttrium as YF₃. Based on electricity costs at a number of aluminum plants, it uses an electricity price of \$30/MWh.

A novel capital cost model developed by Stinn and Allanore⁴² was utilized to estimate the capital costs. This capital cost model, as shown in Eq. 3, has been specifically developed to predict the production-capacity-normalized capital cost of an electrolytic process using its relevant electrochemical operating parameters.

$$\begin{split} C = & \frac{51010}{1 + e^{-3.823*10^{-3}*(T-631)}} P^{0.8} \\ & + \frac{5634000}{1 + e^{-7.813*10^{-3}*(T-349)}} \left(\frac{pzF}{jA\varepsilon M}\right)^{0.9} \\ & + 750000QV^{0.15}N^{0.5} \end{split} \tag{3}$$

In Eq. 3, C is the total direct capital cost in 2018 US dollars, T is the electrolysis temperature in ${}^{\circ}$ C, Pis the installed yearly production capacity in metric tonnes (t), p is the total installed production rate in kg/s, z is the moles of electrons reacting to produce a mole of product, F is the Faraday constant in A/mol, j is the current density in A/m^2 , A is the electrode area in m^2 , ε is the current efficiency, M is the electrolysis product molar mass in kg/mol, Q is the installed power capacity in MW, V is the cell operating voltage, and N is the number of rectifier lines. The Stinn and Allanore cost model does not include the operating expenses or amortization of the capital cost. The authors have verified the estimates of this model by successfully applying it to the cases within the Stinn and Allanore paper.

This capital cost is also verified using a very rough estimate of current costs of new Hall–Héroult cells, rectifier, current bus, and related equipment and buildings, along with a land cost estimate, as described in an interview with Christopher Ritter, Senior Potline Process Engineer at the Century Aluminum smelter in Goose Creek, South Carolina. The capacity of that plant is 200,000 t/a of aluminum, so based on the lower silicon productivity per unit charge, this estimate assumes 160,000 t/a of silicon for the same capital cost and plant footprint.

To estimate the labor costs, we relied on the related data from the same interview regarding the Century Aluminum smelter, ⁴³ again using the labor cost for 200,000 t/a of aluminum production to estimate that for 160,000 t/a of silicon production. At full capacity, that aluminum plant employs 600 cell operators and another 50 in overhead roles, with total labor costs of \$62,800 to \$92,600 per employee. Like the mass balance, the cost model does not include SOM anode costs.

Finite Element Analysis

The FEA of the cell has two goals, namely to compute the effect of the cathode thickness on the current density distribution in the cell layouts shown in Fig. 2, and to estimate the current density and total current more accurately than the 1-D model in the energy balance described above. This model uses COMSOL version 5.5 with the electrochemistry module, which is capable of computing primary, secondary, and tertiary current

distributions. The primary current distribution describes the flow of current in the electrodes and electrolyte based on solutions of the Laplace equation $\nabla \cdot (\sigma \nabla \Phi) = 0$, where σ is the electrical conductivity and Φ is the electrical potential. This assumes that the reaction kinetics and mass transfer are very fast.

Considering a plant-scale electrolysis cell, cathodes are present in the form of slabs with cylindrical anodes, as shown in Fig. 2. The geometry considered here includes one-quarter of a SOM anode, and half of the thickness of the cathode, with a width of half the anode center spacing (3 cm in this case). This is the smallest primitive cell for which the current density distribution is similar to that of most of the anodes and most of the cathode surface. For the model, the nickel current collector is assumed to have the same thickness (2 mm) as the YSZ SOM.

The electrodes are immersed in molten salt electrolyte with the aforementioned composition of CaF₂-MgF₂-YF₃-CaO-SiO₂, whose temperature-dependent conductivity is described by Villalón.³¹ The FEA model uses a subset of this geometry, as shown in Fig. 3. The anode current collector material is

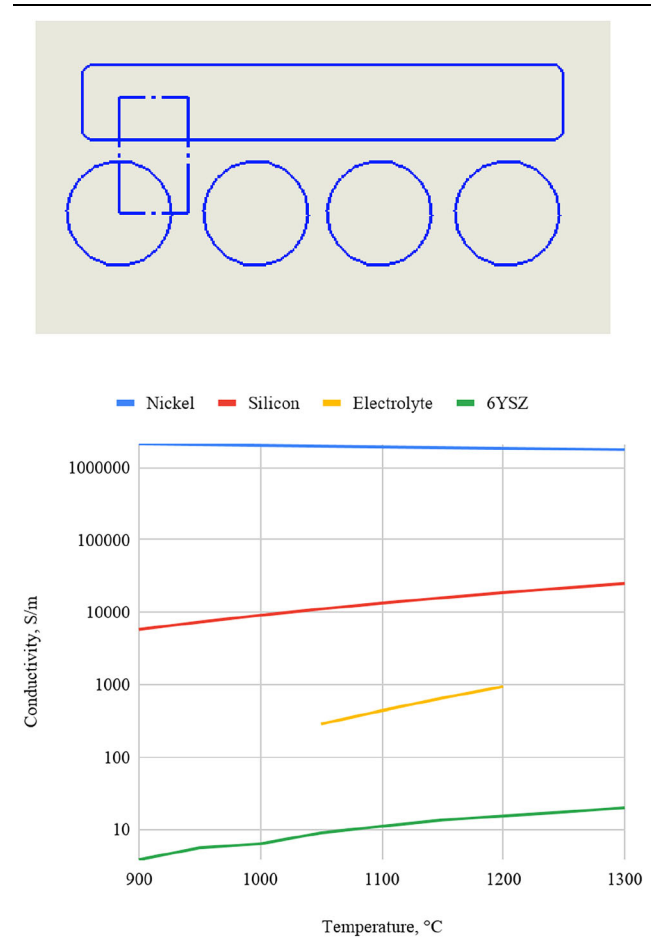


Fig 3. Top-view schematic of the FEA domain geometry (dashed line) relative to a slab cathode and cylindrical anodes shown in Fig. 2 (top), temperature-dependent conductivities of cell materials nickel, pure silicon, molten salt electrolyte, and 6YSZ (bottom).

nickel inside a YSZ solid electrolyte closed-end tube, and the cathode is solid silicon; their conductivities are found in literature 40,44-46 and shown in Fig. 3. As that figure shows, nickel and silicon have far higher conductivities than the liquid and solid electrolytes, so the electrode resistance can almost be neglected. The molten salt electrolyte density was estimated based on the temperature-dependent molar volumes of CaF₂ and MgF₂, 47 which are its main constituents.

The COMSOL electrochemistry module is used to implement the FEA model and estimate the primary current density distribution. The mesh used is a "fine" free-sized tetrahedral mesh defined using COMSOL's physics-based automatic meshing algorithm. The maximum mesh element size is 0.09 m and the minimum mesh element size is 0.0162 m for all three models. The total number of elements approaches 63,000, including domain elements, boundary elements, and edge elements in all three cases. A grid independence test is performed by reducing the mesh size to a maximum mesh element size of 0.0495 m and a minimum mesh element size of 0.0046 m with a curvature factor of 0.4, using the "finer" meshing option in COMSOL.

RESULTS

Techno-economic Modeling

Figure 4 shows the results for the mass and energy balances as follows: The molten salt electrolyte input and compositions are described above, and the output flow rate is slightly higher than the input flow rate due to the incorporation of silica and alumina from the raw material. Every 100 kg Si produced requires 215.4 kg SiO₂. With 99.8% pure SiO₂ containing 0.1 wt.% Al₂O₃, the bath cost to regulate the alumina concentration in the electrolyte at 1 wt.% (a rough estimate of bath purity required for high product purity) amounts to about 59% of the SiO₂ cost. Table I presents the flow rate and cost of each material, not including anode materials, with a total annual cost of just over \$82 million. Note that it is likely possible to separate aluminum from waste fluoride electrolyte via physical, electrochemical, or hydrometallurgical means, and recycle the bath at lower cost than purchasing new material; this analysis does not assume any such activity. For verification, note that the 1 wt.% target alumina concentration in the bath is ten times higher than the 0.1 wt.% concentration in the entering raw material, so the bath must be removed (and a new bath added) at one-tenth of the rate of silica raw material for aluminum to be in balance.

The energy balance shows that the high resistance in the molten salt electrolyte and YSZ solid electrolyte result in a cell potential of V = 3 V to 5 V, and excess thermal energy for a self-heating cell at temperatures below 1200° C. At 1100° C, the total cell voltage is estimated to be 3.37 V, not including the concentration polarizations in the molten salt

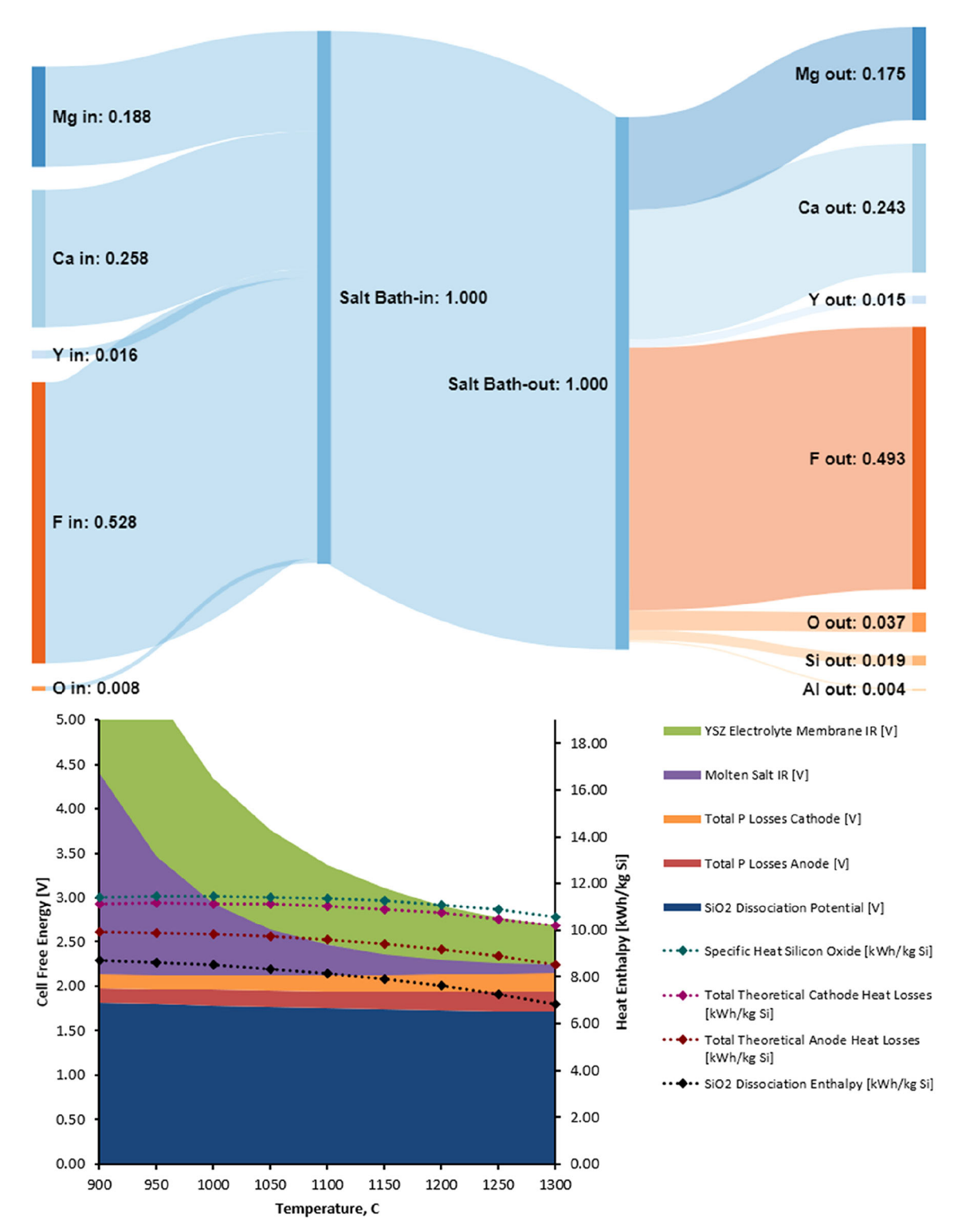


Fig 4. Mass balance of molten salt electrolyte input and output compositions (above), and energy balance (below) showing temperature-dependent electrical energy inputs (stacked solid regions) and thermal energy use (stacked dashed lines).

boundary layers adjacent to the anode and cathode. Of that, 0.190 V represents the ohmic loss in each electrode, which minimizes the total ohmic and thermal losses, so the total ohmic overpotential in the electrodes is 0.38 V, leaving an internal cell

voltage of 4.24 V. At a total voltage drop of 3.37 V, the energy use is 12.88 kWh/kg Si at perfect current efficiency; at 90% current efficiency, this would be 14.3 kWh/kg Si, which is within the 13 kWh/kg to 15 kWh/kg energy use range that is typical for modern

Raw material	Annual use (t)	Price, US\$/t	Total cost, US\$
$\overline{\mathrm{SiO}_2}$	344,000	150	51,600,000
$ m Mgar{F}_2$	18,800	1000	18,800,000
CaF_2	18,800	400	7,520,000
Y_2O_3	800	5000	4,000,000
CaO	600	150	90,000
Total	383,000		82,010,000

Table I. Flow rates and costs of input materials for 160,000 t of silicon production

aluminum smelters. The plant's electrical energy consumption is 2.29 TWh/a, at a cost of \$68.6 million/a. Again based on the aluminum plant example, 43 annual nonelectricity utility costs are about \$13 million/a, so this estimate was added to the utility costs here as well.

For a 160,000 t/a silicon plant, the estimated labor cost for 600 operators and 50 overhead workers, costing \$92,634/a and \$63,800/a, respectively, is \$58.8 million/a. Other overhead and miscellaneous costs are estimated at 25% of raw material, electricity and other utility, and labor costs, coming to \$59.6 million/a. The estimated annual operating costs thus total \$279.0 million/a, i.e., \$1.74/kg silicon product, with the breakdown shown in Fig. 5.

The total capital cost estimated using the cost model developed by Stinn and Allanore is \$1.68 billion, which is around \$10,500 per t/a of production. This estimation is independent of aluminum production by Hall–Héroult cells and only relies on the Si-related operating parameters as explained before. To verify this capital cost model, we used Eq. 3 to estimate the capital cost of aluminum production using the available related operating parameters in the Stinn and Allanore paper. The results were compared with the capital cost of several different aluminum production capacities and found that the estimations by the cost model are very close to the reported numbers.

To verify the silicon plant capital cost estimate, an aluminum industry estimate ⁴³ puts the rough cost of electrolysis cells, rectifiers, raw material distribution, gas scrubbing, and other auxiliary equipment for 200,000 t/a aluminum production at \$1.3 billion. As described above, this corresponds to the amount of current required for 160,000 t/a of silicon production. Land cost is estimated at \$32.5 million, bringing the total capital cost estimate to \$1.33 billion. This is nearly 20% below the estimate using the Stinn and Allanore model, and provides some rough verification of that model, but this only considers fixed capital investment, whereas Stinn and Allanore consider all of the components of total capital investment.

The finance model assumes that 10% of this capital investment is spent in year 1, 60% in year 2, and 30% in year 3. Production reaches 50% of capacity in years 3 and 4, and 100% starting in year

5. Figure 5 shows the cash flows and accumulation under two scenarios. In the first, the silicon sale price is a constant \$3.00/kg, and costs are constant; in this case the initial investment is paid back in about 11 years. In the second, the silicon sale price starts at \$4.00/kg and declines by 2%/a, while costs increase 2%/a; in this case, the initial investment is paid back in 9 years, but further reductions in input costs (energy, labor, and raw materials) would be required to maintain profitability well beyond year 20.

Finite Element Analysis

Figure 6 shows the calculated primary current density distribution in the form of current "streamlines" for four cathode slab thicknesses from 2 cm to 8 cm (half-thickness from 1 cm to 4 cm). The current density is roughly uniform over the anode-SOM interface, and for most of the cathode at higher thickness, although current concentrates at the bottom of the cathode. Figure 6 shows the electrical potential distribution throughout the model domain. This model calculates the current for onequarter of an anode, so multiplying by four gives the total anode current, and dividing the model output by the cathode area in the model (360 cm²) gives the average cathode current density. The total current per anode and the average current density on the cathode surface are shown versus The cathode thickness in Table II. At 4.0 cm cathode thickness, the anode current calculated using COMSOL's "finer" mesh option is 1.3% below that obtained using the "fine" option applied for most of the results, indicating reasonable grid independence.

DISCUSSION

In the mass balance, two mechanisms promote purification: low partition coefficients in silicon, and electronegativity, which leaves most of the bath elements in the bath. However, it is possible that more-electronegative elements could accumulate in the bath, and those with higher partition coefficients such as phosphorus could contaminate the product. In this case, it should be straightforward to remove electronegative elements electrolytically by using a pre-electrolysis step as described in Ref. 35. Boron is the most problematic element, as its electronegativity is similar to that of silicon and it

Annual Operating Cost Breakdown

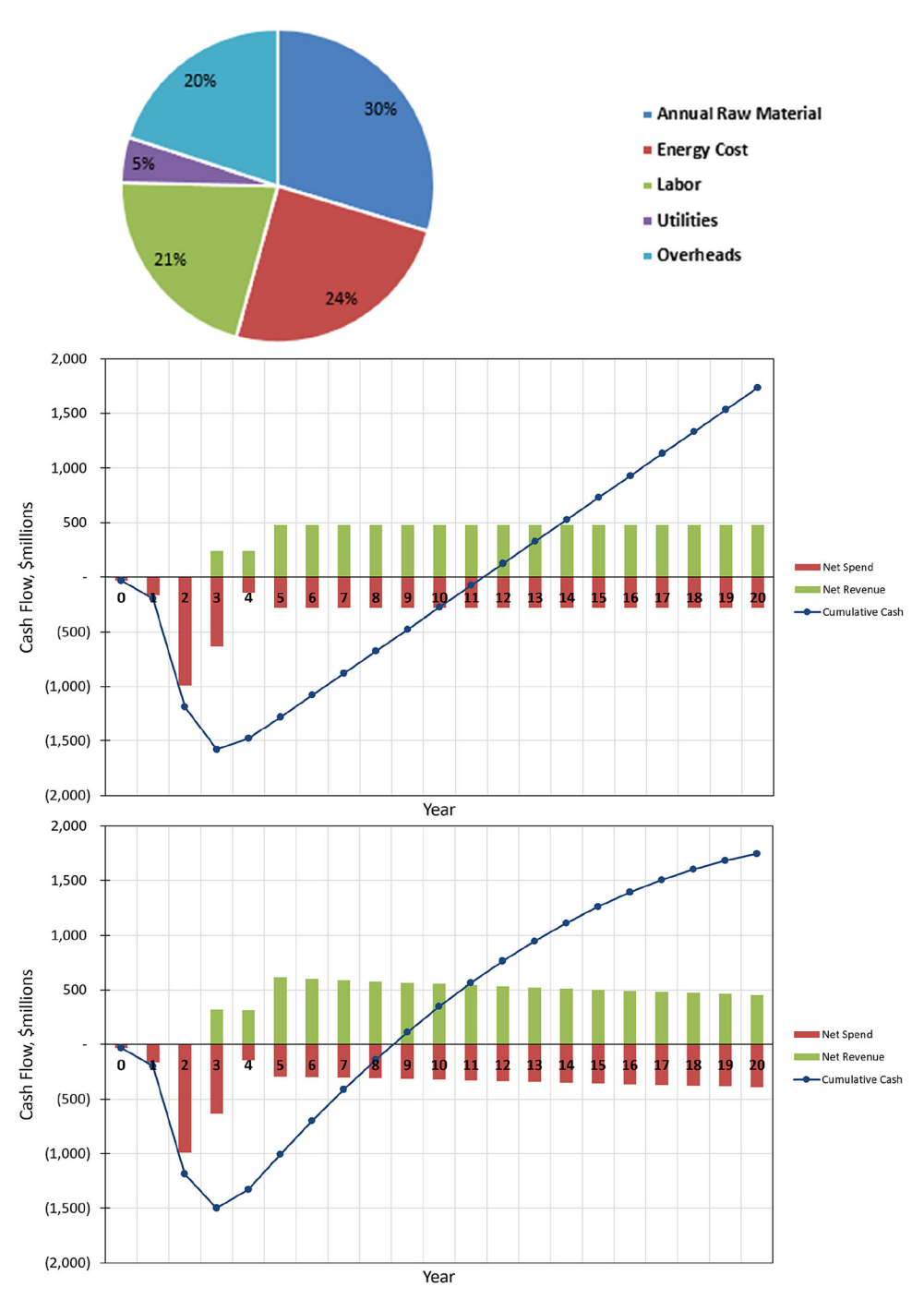


Fig 5. Cost model results: breakdown of operating costs (top), and total annual costs, revenues, and cumulative cash using \$3.00/kg starting silicon price with no changes (center), and \$4.00/kg starting price with 2% price reduction and 2% cost increases (bottom).

has a high partition coefficient, although in this bath it may volatilize as BF_3 . It is not clear whether the purity of the product obtained from this process will be sufficient for solar cells.

The cost comparisons with aluminum are compelling, as the prospect of solar silicon at aluminum price could be very interesting to the PV industry,

but not straightforward. The contributions to this model include the raw material cost and purity (silica is about 60% cheaper per tonne with higher purity), energy cost (the voltage and energy cost per kilogram are similar to aluminum with inert anodes), and productivity (lower productivity per kAh charge, thus lower plant production for the

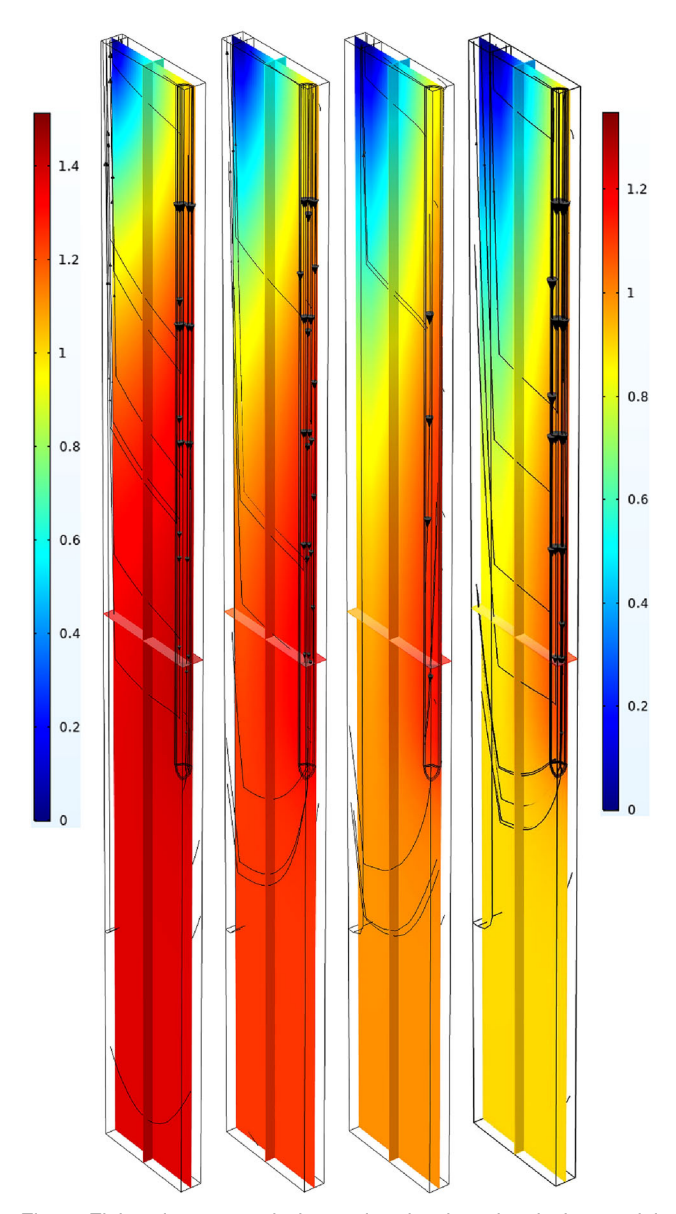


Fig 6. Finite element analysis results showing electrical potential distribution (background colors) and primary current density distribution streamlines (black) for 2-cm-, 4-cm-, 6-cm-, and 8-cm-thick cathodes (1 cm, 2 cm, 3 cm, and 4 cm half-thicknesses in the model). The quarter anode is in the foreground of each domain, while the half-thickness cathode section is in the back. The left scale applies to the left two plots, and the right scale to the right two plots (Color figure online).

same cell current and number of cells). The other major cost category, which is labor, is more complicated. Product removal from cells is complex compared with Hall–Héroult cells, as disconnecting and replacing at least 20 cathodes, preparation and quality assurance, and creating new slabs to go back into the cell is more convoluted than siphoning out liquid aluminum. That being said, cathode changes should take place about once a week versus daily, and the zirconia anodes will likely last longer than carbon anodes. Thus, the silicon labor cost might be higher, but not sufficiently so to raise the total operating cost significantly.

The capital cost as modeled by Stinn and Allanore ⁴² is a rough estimate accurate to within about 10% to 15% of data used in its development. It is also very sensitive to the bus and cell current. The capital cost estimate of above \$1.68 billion assumed 234 cells with a current of 300 kA. If such large cells are not possible, for example with 200 kA current and 351 cells, the estimated capital cost rises to \$2.04 billion; if the cell current is 100 kA with 702 cells, then the estimated capital cost rises still further to \$3.08 billion.

One factor that could raise the operating cost significantly is the zirconia anodes. When not polarized, the corrosion rate for this bath composition is unmeasurably low,³⁰ but the corrosion rate and lifetime when polarized, or when the composition fluctuates during operation, is uncertain at this time.

CONCLUSION

A techno-economic model and finite element analysis are used to examine the feasibility of molten salt electrolysis with YSZ SOM anodes for production of solid silicon for PV applications, with the following results:

- The mass balance determines that it takes a significant amount of new electrolyte to prevent accumulation of impurities, particularly alumina, in the electrolyte; that additional electrolyte can cost as much as 10% of the silica.
- The energy balance indicated that a self-heating cell at 1100°C should operate at about 3.4 V plus a small concentration overpotential, and would

Table II. Calculated cell current per anode and average current density at the cathode-electrolyte interface

Cathode thickness (cm)	Anode current (A)	Average cathode current density (A/cm ²)
2.0	95.9	0.066
4.0	133.0	0.092
6.0	156.0	0.108
8.0	173.8	0.121

- consume 14.3 kWh/kg silicon product. Although representing the largest component of the operating cost, this is far less energy than the Siemens process, which uses more than 150 kWh/kg, or the Elkem process, which uses just below 90 kWh/kg.
- The cost analysis included raw materials, energy, labor, and a contingency estimated total operating cost of \$1.74/kg Si product, with a capital cost just under \$1.7 billion for a 160 kt/a plant. The payback period would depend on the polysilicon sale price, changes in price, and input costs: at \$3/kg with no changes, the initial investment would be paid back in about 11 years. Such a plant would supply about one-third of the world's current PV polysilicon market.
- The total current estimated using the finite element analysis was very consistently with the 1-D energy balance model. The FEA results indicated that, at 1100°C, a 1.2-m-high vertical solid silicon cathode can achieve a mostly uniform primary current density distribution if at least 4 cm thick (with 2 cm half-thickness). This model will inform the electrode design and operation characteristics.

ACKNOWLEDGMENTS

This material is based upon work supported by the US Department of Energy's Office of Energy Efficiency and Renewable Energy (EERE) under the Solar Energy Technologies Office Award No. DE-EE0008988 and by the US National Science Foundation under Award Nos. 1937818 and 1829089. This research was performed using computational resources supported by the Academic and Research Computing group at Worcester Polytechnic Institute.

CONFLICT OF INTEREST

The authors declare that they have no conflict of interest.

ELECTRONIC SUPPLEMENTARY MATERIAL

The online version of this article (https://doi.org/ 10.1007/s11837-020-04468-y) contains supplementary material, which is available to authorized users.

REFERENCES

- 1. S.A. Mann, M.J. de Wild-Scholten, V.M. Fthenakis, W.G.J.H.M. van Sark, and W.C. Sinke, Prog. Photovolt. Res. Appl. 22, 1180 (2014).
- M. Osborne, "Explosion at Mitsubishi polysilicon plant in Japan causes deaths" PV Tech (2014). https://www.pv-tech.

- $org/news/explosion_at_mitsubishi_polysilicon_plant_in_jap$ an_causes_deaths. Accessed July 2020.
- 3. M. Pace, "Final investigation determines Wacker explosion out of company's control" Chatt. Times Free Press (2018). h ttps://www.timesfreepress.com/news/breakingnews/story/20 18/jul/05/final-investigation-wacker-explosion/474431/. Accessed July, 2020.
- 4. n.a. "Polysilicon Shortage: Production Solar panels in Danger" BetterWorldSolutions—Neth. (2018). https://www.bette rworldsolutions.eu/rawmaterial-shortage-production-solarpanels-danger/. Accessed July 2020. T. Buonassisi, A.A. Istratov, M.A. Marcus, B. Lai, Z. Cai,
- S.M. Heald, and E.R. Weber, Nat. Mater. 4, 676 (2005).
- W.O. Filtvedt, M. Javidi, A. Holt, M.C. Melaaen, E. Marstein, H. Tathgar, and P.A. Ramachandran, Sol. Energy Mater. Sol. Cells 94, 1980 (2010).
- A. Ramos, W.O. Filtvedt, D. Lindholm, P.A. Ramachandran, A. Rodríguez, and C. del Cañizo, J. Cryst. Growth 431, 1
- S. Nichol, U.S. Patent 7,727,503 (1 June 2010).
- Y. Ren, S. Ueda, and K. Morita, A.C.S. Sustain. Chem. Eng. 7, 20107 (2019).
- 10. L.A.V. Teixeira and K. Morita, ISIJ Int. 49, 783 (2009).
- 11. K. Morita and T. Yoshikawa, Trans. Nonferrous Met. Soc. China 21, 685 (2011).
- 12. E. Olsen and S. Rolseth, Metall. Mater. Trans. B 41, 295 (2010).
- Y.-Q. Lai, M. Jia, Z.-L. Tian, J. Li, J.-F. Yan, J.-G. Yi, Z.-G. Wang, and Y.-X. Liu, Metall. Mater. Trans. A 41, 929 (2010).
- K. Johansen, D.R. Sadoway, B. Myhre, M. Engvoll, and K. Engvoll, 7,901,561 (8 March 2011).
- G.M. Haarberg, in TMS Middle East Mediterr. Mater. Congr. Energy Infrastruct. Syst. MEMA 2015 (TMS, 2015),
- p. 6. T. Nohira, in *Encycl. Appl. Electrochem.*, edited by G. Kreysa, K. Ota, and R. F. Savinell (Springer New York, New York, NY, 2014), pp. 1963-1966.
- E. Juzeliunas and D.J. Fray, Chem. Rev. 120, 1690 (2020).
- 18. K. Yasuda, T. Nohira, K. Amezawa, Y.H. Ogata, and Y. Ito, J. Electrochem. Soc. 152, D69 (2005).
- X. Jin, P. Gao, D. Wang, X. Hu, and G.Z. Chen, Angew. Chem. Int. Ed. 43, 733 (2004).
- U. Cohen, J. Electron. Mater. 6, 607 (1977).
- D. Elwell and G.M. Rao, J. Appl. Electrochem. 18, 15 (1988).
- J.T. Moore, T.H. Wang, M.J. Heben, K. Douglas, and T.F. Ciszek, in Conf. Rec. Twenty Sixth IEEE Photovolt. Spec. Conf.—1997 (IEEE, Anaheim, CA, USA, 1997), pp. 775–778.
- 23. K. Grjotheim, K. Matiaśovský, P. Fellner, and A. Silný, Can. Metall. Q. 10, 79 (1971).
 T. Oishi, M. Watanabe, K. Koyama, M. Tanaka, and K.
- 24. Saegusa, J. Electrochem. Soc. 158, E93 (2011).
- 25. G. Bøe, K. Grjotheim, K. Matiašovský, and P. Fellner, Can. Metall. Q. 10, 281 (1971).
- G. Bøe, K. Grjotheim, K. Matiašovský, and P. Fellner, Can. Metall. Q. 11, 463 (1972).
- G.M. Haarberg, T. Kato, Y. Norikawa, and T. Nohira, ECS Trans. 89, 29 (2019).
- Y. Ma, A. Ido, K. Yasuda, R. Hagiwara, T. Homma, and T. Nohira, J. Electrochem. Soc. 166, D162 (2019).
- J. Xu, B. Lo, Y. Jiang, U. Pal, and S. Basu, J. Eur. Ceram. Soc. 34, 3887 (2014).
- J. Guo, T. Villalon, U. Pal, and S. Basu, J. Am. Ceram. Soc. 30. 101, 3605 (2018).
- T. Villalón Jr., Zero-Direct Emission Silicon Production via Solid Oxide Membrane Electrolysis (Ph.D.: Boston University, 2018).
- U.B. Pal, D.E. Woolley, and G.B. Kenney, JOM 53, 32 (2001).
- U.B. Pal and A.C. Powell, JOM 59, 44 (2007).
- X. Ma, T. Yoshikawa, and K. Morita, J. Cryst. Growth 377, 192 (2013).

- A.C. Powell and S.J. Derezinski, U.S. Patent 8,460,535 (11 June 2013).
- D. Matuszak, ARPA-E METALS Tool (Department of Energy: U.S, 2013).
- K.I. Vatalis, G. Charalambides, and N.P. Benetis, Procedia Econ. Finance 24, 734 (2015).
- A. Powell and S. Pati, in CFD Model. Simul. Mater. Process., edited by L. Nastac, L. Zhang, B.G. Thomas, A. Sabau, N. El-Kaddah, A.C. Powell, and H. Combeau (John Wiley & Sons, Inc., Hoboken, NJ, USA, 2012), pp. 57–64.
- M.W. Chase, NIST-JANAF Thermochemical Tables, 4th ed. (National Institute of Technology, Gaithersburg, Maryland, USA, 1996).
- A. Krishnan, Solid Oxide Membrane Process for the Direct Reduction of Magnesium from Magnesium Oxide (Ph.D.: Boston University, 2006).
- Z.R. Hesabi, M. Mazaheri, and T. Ebadzadeh, J. Alloys Compd. 494, 362 (2010).

- 42. C. Stinn and A. Allanore, *Electrochem. Soc. Interface* 29, 44 (2020).
- C. Ritter, Interview regarding operation and economics of Century Aluminum's Goose Creek smelter (2020).
- A. Cezairliyan and A.P. Miiller, Int. J. Thermophys. 4, 389 (1983).
- 45. M.C.H.M. Wouters, H.M. Eijkman, and L.J. van Ruyven, *Philips Res. Repts.* 31, 278 (1976).
- S. Fan, G. Plascencia, and T. Utigard, Can. Metall. Q. 47, 509 (2008).
- D.E. Holcomb and S.M. Cetiner, An Overview of Liquid-Fluoride-Salt Heat Transport Systems (Oak Ridge National Laboratory, 2010).

Publisher's Note Springer Nature remains neutral with regard to jurisdictional claims in published maps and institutional affiliations.